Queries to the Author

When you submit your corrections, please either annotate the IEEE Proof PDF or send a list of corrections. Do not send new source files as we do not reconvert them at this production stage.

Authors: Carefully check the page proofs (and coordinate with all authors); additional changes or updates WILL NOT be accepted after the article is published online/print in its final form. Please check author names and affiliations, funding, as well as the overall article for any errors prior to sending in your author proof corrections. Your article has been peer reviewed, accepted as final, and sent in to IEEE. No text changes have been made to the main part of the article as dictated by the editorial level of service for your publication.

Per IEEE policy, one complimentary proof will be sent to only the Corresponding Author. The Corresponding Author is responsible for uploading one set of corrected proofs to the IEEE Author Gateway

Q1. Please provide index term for this article.
Q2. Please confirm or add details for any funding or financial support for the research of this article.
Q3. Please provide page range for Ref. [10].
Q4. Please provide year for Refs. [15], [16].

Modeling Movement-Induced Errors in AC Electromagnetic Trackers

Mutaz Tuffaha, Øyvind Stavdahl, and Ann-Katrin Stensdotter

Abstract—Error analysis of electromagnetic motion tracking systems is of growing interest to many researchers. Under sensor movement, it is logical to presume that the error in position and orientation measurements will increase due to the linearization used in the algorithms, among other reasons. In this article, we analyze theoretically the error, that results from linearization, in position measurement of the Polhemus tracking system for a moving sensor. We derive formulas to estimate this error in terms of the sensor position and speed. Then, we verify these formulas by numerical simulations.

Q1 **Index Terms**—.

1 INTRODUCTION

Because they do not require a direct line of sight, *electromagnetic motion tracking systems* (EMTS) have been used in many research arenas such as, inter alia, computer-assisted medical interventions [1], Biomechanical movements analysis [2] and [3], Robotics [4], virtual/augmented/mixed reality and simulators [5] and [6]. Usage of EMTS in these contexts range from capturing the geometry and movements of the real-world objects and actors for geometric modeling purposes to intuitive use interfaces for advanced visualization applications.

Since the pioneering work in [7], many papers and patents have been written in which the authors have been trying to exploit magnetic field theory to track moving objects. Simultaneously, many manufacturers have been competing to introduce EMTS. For surveys on the various techniques and manufacturers of EMTS, the reader is advised to see e.g., [1], [5], or [8].

On the other hand, many researchers have been interested in investigating the accuracy of such systems. The authors in [1] classify the errors of EMTS into *static* and *dynamic*. Static errors are encountered when the sensor is fixed, while dynamic errors arise due to sensor movement [1]. The sources of the errors in such systems can be classified, also according to [1] into: Inherent System Errors (such as noise of the field generator), Field Distortion Errors (resulting from interference with ferromagnetic materials or electromagnetic fields other than the field generated by the system in the surrounding), and Motion-Induced Errors (resulting from the motion of the sensor).

Because manufacturers usually prefer to keep the details of their products covert, and because the algorithms and techniques used in EMTS span a wide range of theories and inventions, investigating the accuracy of such systems theoretically would be very challenging. Furthermore, the complexity of the analysis multiplies as the sources of errors, mentioned earlier, vary in nature and contribution. That is why the researchers prefer the experimental study of the accuracy over the theoretical analysis. Experiments can be carried out by using special apparatuses or phantoms, and then the measurements are usually compared with a specific gold standard. The phantoms can be stationary if the static accuracy is under investigation such as a plate or pegboard [9], while moving phantoms such as a pendulum [10] or a moving plate [11] are used to investigate the dynamic accuracy.

To our best knowledge, very few studies on the theoretical analysis were published. For example, the authors in [12] showed, theoretically and experimentally, that the error due to electrical fields and nearby metals increases as the fourth power of the distance from the transmitter, but they considered stationary sensors only. Another example can be found in [13] where the author proposed an algorithm to track objects through-the-earth such as in drill guidance and mine rescue. Further, he did some sensitivity analysis of his own algorithm and found some limits on the error in position and orientation errors, but he also did not consider the dynamics of the sensor [13].

We believe that it is important to study and analyze the mathematical algorithm used by a particular EMTS, especially when it comes to dynamic accuracy of that specific EMTS. Most of the algorithms used by manufacturers depend on some kind of linearization to determine the position and orientation, in other words, six *degrees of freedom* (DOF) of the moving sensor. This linearization by itself introduces some error, especially as the speed increases.

- *Mutaz Tuffaha is with Indra Navia AS, NO-1383 Asker, Norway. E-mail: mutaz.tuffaha@indra.no.*
- *Øyvind Stavdahl is with the Department of Engineering Cybernetics, Faculty of Information Technology, Mathematics and Electrical Engineering, Norwegian University of Science and Technology (NTNU), NO-7491 Trondheim, Norway. E-mail: oyvind.stavdahl@ntnu.no.*
- *Ann-Katrin Stensdotter is with the Department of Neuromedicine and Movement Science, Faculty of medicine and Health Sciences, Norwegian University of Science and Technology (NTNU), NO-7491 Trondheim, Norway. E-mail: ann-katrin.stensdotter@ntnu.no.*

Manuscript received 6 May 2019; revised 9 Aug. 2020; accepted 20 Aug. 2020. Date of publication 0 . 0000; date of current version 0 . 0000.
(Corresponding author: Mutaz Tuffaha.)
Recommended for acceptance by K. Kiyokawa.
Digital Object Identifier no. 10.1109/TVCG.2020.3019700

Obviously, the linearization is not the only source of error, and perhaps not the most influential one. However, it is certainly a source of error that needs to be quantified and taken into consideration when analyzing the error of EMTS, and this is the topic of this paper.

Some of the current authors participated in a previous work on head stabilization [14], and they used LIBERTY system [15] from Polhemus [16], in their experiments. Thus, dynamic accuracy of this EMTS is of particular interest. Actually, Polhemus was one of the first companies to introduce EMTS based on the work in e.g., [17] and [18]. Fortunately, the algorithm described in [17] is still used by Polhemus after almost 40 years. The technical support in Polhemus confirmed that the basic concept of tracking is still as described in [17], but of course over all these years they have been developing and improving their system by using the most cutting-edge techniques in electronics and signal processing.

So, in this work we theoretically investigate the dynamic error in position and orientation measurements by Polhemus EMTS according to their published algorithm in [17]. We further derive formulas to estimate the error in position measurements at fixed orientation in terms of the position and speed of the sensor in spherical coordinates. Then, we show by simulations that the proposed formulas are accurate even when the orientation changes, as long as the rates of change of the Euler angles are not large. It is worth mentioning here that we are investigating the error due to linearization only that results from the motion of the sensor. Thus, we do not consider the field distortion errors that result from the interference with ferromagnetic materials or other electromagnetic fields. We do all our analysis in spherical coordinates, but extending the proposed formulas to Cartesian coordinates would not be problematic.

The proposed formulas show that this error increases or accumulates with time systematically as the sensor moves, even if the speed is constant. In addition, those formulas can predict the singularities around which the error may explode. Our simulations confirm those conclusions, as will be shown later.

The importance of the proposed formulas is twofold. First, they are of great interest to the researchers who are interested in error analysis of EMTS and the manufacturers for development purposes. Moreover, the proposed error model can be used for any system that uses this type of linearization. The paper is organized as follows. In the subsequent section we present a summary of the basic algorithm used by Polhemus, as explained in [17], and we state the problem. In Section 3, we derive the proposed formulas that can be used to quantify the error in position measurements assuming fixed orientation. In Section 4, we investigate the error in orientation measurements and we discuss the influence of changing the orientation on the proposed formulas. In the last section we draw our conclusions.

2 The Basic Algorithm and Problem Statement

In this section, we summarize the basic algorithm used by Polhemus system, as described in [17]. This algorithm depends on the orthogonal rotational matrices given in Table 1.

TABLE 1
List of Rotation Matrices

About	Position	Orientation
z-axis	$\mathbf{T}_\alpha = \begin{bmatrix} \cos\alpha & \sin\alpha & 0 \\ -\sin\alpha & \cos\alpha & 0 \\ 0 & 0 & 1 \end{bmatrix}$	$\mathbf{T}_\psi = \begin{bmatrix} \cos\psi & \sin\psi & 0 \\ -\sin\psi & \cos\psi & 0 \\ 0 & 0 & 1 \end{bmatrix}$
y-axis	$\mathbf{T}_\beta = \begin{bmatrix} \cos\beta & 0 & -\sin\beta \\ 0 & 1 & 0 \\ \sin\beta & 0 & \cos\beta \end{bmatrix}$	$\mathbf{T}_\theta = \begin{bmatrix} \cos\theta & 0 & -\sin\theta \\ 0 & 1 & 0 \\ \sin\theta & 0 & \cos\theta \end{bmatrix}$
x-axis	$\mathbf{T}_\gamma = \begin{bmatrix} 1 & 0 & 0 \\ 0 & \cos\gamma & \sin\gamma \\ 0 & -\sin\gamma & \cos\gamma \end{bmatrix}$	$\mathbf{T}_\phi = \begin{bmatrix} 1 & 0 & 0 \\ 0 & \cos\phi & \sin\phi \\ 0 & -\sin\phi & \cos\phi \end{bmatrix}$

The source has three orthogonal coils, so three distinct excitation states can be used, as follows:

$$\mathbf{S}_1 = \begin{bmatrix} 1 \\ 0 \\ 0 \end{bmatrix}, \mathbf{S}_2 = \begin{bmatrix} 0 \\ 1 \\ 0 \end{bmatrix} \text{ and } \mathbf{S}_3 = \begin{bmatrix} 0 \\ 0 \\ 1 \end{bmatrix}, \tag{1}$$

where each one describes the excitation in one coil. Assuming that the three coils of the source are identical, the output of the source can be represented by a vector $\mathbf{f}_1 = [f_{1x}, f_{1y}, f_{1z}]^T$. In this model, the source and the sensor are considered as point source and point sensor. Now, if the sensor is located at position $(\rho, \alpha_1, \beta_1)$ relative to the source spherical coordinate frame i.e., the coordinate system centered at the source with its $x-$, $y-$ and $z-$ axes are aligned with the fixed source coils, the output of an equivalent source whose $x-$ axis is aligned with the line connecting the sensor and the source can be described by [17]:

$$\mathbf{f}_2 = \mathbf{T}_{\beta_1}\mathbf{T}_{\alpha_1}\mathbf{f}_1. \tag{2}$$

Because the wavelength of the used excitation signal is much longer than the distance between the source and the sensor, near-field components are only considered. Hence, the output of the source coils at the sensor position can be modeled by [17]:

$$\mathbf{f}_3 = \frac{C}{\rho^3}\mathbf{S}\mathbf{f}_2, \tag{3}$$

where C is a constant depends on the magnetic coupling between the source and the sensor, and $\mathbf{S}$ describes that coupling and is given by [17]:

$$\mathbf{S} = \begin{bmatrix} 1 & 0 & 0 \\ 0 & -\frac{1}{2} & 0 \\ 0 & 0 & -\frac{1}{2} \end{bmatrix}. \tag{4}$$

Then, to make the sensor output oriented with the source frame, one needs to rotate the sensor output in reverse direction to obtain a zero-oriented output as [17]:

$$\mathbf{f}_4 = \mathbf{T}_{-\alpha_1}\mathbf{T}_{-\beta_1}\mathbf{f}_3. \tag{5}$$

Finally, assuming that the sensor orientation can be described by three angles $(\psi_1, \theta_1, \phi_1)$ from the sensor frame, which is now aligned with the source frame, the sensor output after inserting (2), (3) and (5) is given by [17]:

$$\begin{aligned}\mathbf{f}_5 =&\mathbf{T}_{\phi_1}\mathbf{T}_{\theta_1}\mathbf{T}_{\psi_1}\mathbf{f}_4\\ =&\frac{C}{\rho^3}\mathbf{T}_{\phi_1}\mathbf{T}_{\theta_1}\mathbf{T}_{\psi_1}\mathbf{T}_{-\alpha_1}\mathbf{T}_{-\beta_1}\mathbf{S}\mathbf{T}_{\beta_1}\mathbf{T}_{\alpha_1}\mathbf{f}_1\\ =&\frac{C}{\rho^3}\mathbf{Q}\mathbf{f}_1.\end{aligned} \tag{6}$$

The sensor also has three coils, and thus three measurements can be taken from the sensor. We represent them here by the following three row vectors:

$$\mathbf{M}_1^T = \begin{bmatrix}1\\0\\0\end{bmatrix}, \mathbf{M}_2^T = \begin{bmatrix}0\\1\\0\end{bmatrix} \text{ and } \mathbf{M}_3^T = \begin{bmatrix}0\\0\\1\end{bmatrix}. \tag{7}$$

This algorithm assumes that the output of each sensor coil corresponding to each excitation state can be distinguished, separately. This means that three different measurements $\mathbf{M}_1\mathbf{f}_5$, $\mathbf{M}_2\mathbf{f}_5$ and $\mathbf{M}_3\mathbf{f}_5$ can be taken for each one of excitation states $\mathbf{S}_1$, $\mathbf{S}_2$ and $\mathbf{S}_3$ when used as inputs for $\mathbf{f}_1$. Thus, we end up with nine different measurements at each time instant which are more than enough to determine the position $(\rho, \alpha_1, \beta_1)$ and the orientation $(\psi_1, \theta_1, \phi_1)$, or the so-called 6 DOF. In practice, this requires some sort of multiplexing (time, frequency or similar) or modulation to distinguish the outputs of the sensor coils for each excitation state. Unfortunately, the authors in [17] did not specify which type of multiplexing the company uses. Let us, from here on, presume that the nine measurements can be taken simultaneously, or at least the time gaps between those measurements (assuming time multiplexing) are so small compared to the updating time, as will be explained later. Obviously, the transformation matrix $\mathbf{Q} \in \mathbb{R}^{3\times 3}$ in (6) is highly nonlinear because of the many products of the sines and cosines of different angles. Hence, there could be no way to find the six unknowns even with the nine equations from the nine measurements. Instead, the authors in [17] proposed to linearize this transformation by what they called *previous measurement* technique. Actually, the idea is so intuitive. The nine measurements described above are taken and updated at every time step ΔT_u. In this technique, it is assumed that the estimates of the position $(\hat{\rho}, \hat{\alpha}_1, \hat{\beta}_1)$ and the orientation $(\hat{\psi}_1, \hat{\theta}_1, \hat{\phi}_1)$ at the previous time step are known. Then, the position and orientation at the current time step can be determined as follows. The output of the source at the current time step $\mathbf{f}_1$ can be determined from the output of the source at the previous time step $\mathbf{f}_0$ by [17]:

$$\mathbf{f}_1 = \mathbf{T}_{-\hat{\alpha}_1}\mathbf{T}_{-\hat{\beta}_1}\mathbf{f}_0. \tag{8}$$

Similarly, the sensor output $\mathbf{f}_5$ can be rotated in reverse direction to make it zero-oriented based on the previous measurement as [17]:

$$\mathbf{f}_6 = \mathbf{T}_{-\hat{\psi}_1}\mathbf{T}_{-\hat{\theta}_1}\mathbf{T}_{-\hat{\phi}_1}\mathbf{f}_5. \tag{9}$$

Then, the output should be rotated by the previous measured angles to make it aligned with the source again, as [17]:

$$\mathbf{f}_7 = \mathbf{T}_{\hat{\beta}_1}\mathbf{T}_{\hat{\alpha}_1}\mathbf{f}_6. \tag{10}$$

Inserting (8), (9) and (10) in (6), one gets:

$$\mathbf{f}_7 = \frac{C}{\rho^3}\mathbf{R}\mathbf{f}_0, \tag{11}$$

where

$$\begin{aligned}\mathbf{R} =&\mathbf{T}_{\hat{\beta}_1}\mathbf{T}_{\hat{\alpha}_1}\mathbf{T}_{-\hat{\psi}_1}\mathbf{T}_{-\hat{\theta}_1}\mathbf{T}_{\phi_1-\hat{\phi}_1}\mathbf{T}_{\theta_1}\mathbf{T}_{\psi_1-\alpha_1}\mathbf{T}_{-\beta_1}\dots\\ &\dots\mathbf{S}\mathbf{T}_{\beta_1}\mathbf{T}_{\alpha_1-\hat{\alpha}_1}\mathbf{T}_{-\hat{\beta}_1}.\end{aligned} \tag{12}$$

As a matter of fact, the differences between the previous and current measurements of the position and orientation are supposed to be small if the updating time ΔT_u is small enough, and the velocities or rates of change are not so high. Let $\Delta\alpha_1$, $\Delta\beta_1$, $\Delta\psi_1$, $\Delta\theta_1$ and $\Delta\phi_1$, be the differences between the current and previous measurements of the angle $\alpha_1, \dots, \phi_1$, respectively, such that [17]:

$$\Delta\alpha_1 = \alpha_1 - \hat{\alpha}_1, \tag{13}$$

and so on. Note that the incremental angles $\Delta\alpha_1, \dots, \Delta\phi_1$ are measured in the source frame coordinates. However, those incremental angles can also be measured in what the authors in [17] called *tracking* frame coordinates, which is defined by rotations from the source frame by the previously estimated angles $\hat{\alpha}_1$ and $\hat{\beta}_1$. The corresponding incremental changes of the angles in the tracking frame are denoted by $\Delta\alpha_0, \dots, \Delta\phi_0$. By using those definitions, the authors showed that the $\mathbf{R}$ matrix in (12) can be approximated by [17]:

$$\widetilde{\mathbf{R}} = \begin{bmatrix} 1 & \frac{3}{2}\Delta\alpha_0 - \frac{1}{2}\Delta\psi_0 & -\frac{3}{2}\Delta\beta_0 + \frac{1}{2}\Delta\theta_0 \\ \frac{3}{2}\Delta\alpha_0 - \Delta\psi_0 & -\frac{1}{2} & -\frac{1}{2}\Delta\phi_0 \\ -\frac{3}{2}\Delta\beta_0 + \Delta\theta_0 & \frac{1}{2}\Delta\phi_0 & -\frac{1}{2} \end{bmatrix}. \tag{14}$$

As explained before, since the outputs in the three coils of the sensor can be measured for the three excitation states (simultaneously), the nine elements of the $\widetilde{\mathbf{R}}$ matrix can be determined and hence the incremental angles. First of all, assuming that the constant C in (11) is known, the estimate of the distance ρ from the source is obtained from (14) by:

$$\tilde{\rho} = \sqrt{[3]}\frac{C}{2\mathbf{M}_1\mathbf{R}\mathbf{S}_1} = \sqrt{[3]}\frac{-C}{2\mathbf{M}_2\mathbf{R}\mathbf{S}_2} = \sqrt{[3]}\frac{-C}{2\mathbf{M}_3\mathbf{R}\mathbf{S}_3}. \tag{15}$$

Then, the incremental angles measured in the tracking frame can be approximated as follows [17]:

$$\begin{aligned}\widetilde{\Delta\alpha}_0 =&\frac{2\tilde{\rho}^3}{3C}(2\mathbf{M}_1\mathbf{R}\mathbf{S}_2 - \mathbf{M}_2\mathbf{R}\mathbf{S}_1)\\ \widetilde{\Delta\beta}_0 =&\frac{2\tilde{\rho}^3}{3C}(\mathbf{M}_3\mathbf{R}\mathbf{S}_1 - 2\mathbf{M}_1\mathbf{R}\mathbf{S}_3)\\ \widetilde{\Delta\psi}_0 =&\frac{2\tilde{\rho}^3}{C}(\mathbf{M}_1\mathbf{R}\mathbf{S}_2 - \mathbf{M}_2\mathbf{R}\mathbf{S}_1)\\ \widetilde{\Delta\theta}_0 =&\frac{2\tilde{\rho}^3}{C}(\mathbf{M}_3\mathbf{R}\mathbf{S}_1 - \mathbf{M}_1\mathbf{R}\mathbf{S}_3)\\ \widetilde{\Delta\phi}_0 =&\frac{2\tilde{\rho}^3}{C}\mathbf{M}_3\mathbf{R}\mathbf{S}_2 = -\frac{2\tilde{\rho}^3}{C}\mathbf{M}_2\mathbf{R}\mathbf{S}_3.\end{aligned} \tag{16}$$

The next step is to transform the incremental angles from the tracking frame to the source frame. To this end, the authors in [17] showed that:

$$\widetilde{\Delta\alpha}_1 = \frac{\widetilde{\Delta\alpha}_0}{\cos\beta_1} \text{ s.t. } \beta_1 \neq \pm\frac{\pi}{2}, \widetilde{\Delta\beta}_1 = \widetilde{\Delta\beta}_0, \tag{17}$$

and

$$\begin{bmatrix} \widetilde{\Delta\phi}_1 \cos\hat{\theta}_1 \\ \widetilde{\Delta\theta}_1 \\ \widetilde{\Delta\psi}_1 - \widetilde{\Delta\phi}_1 \sin\hat{\theta}_1 \end{bmatrix} = \mathbf{T}_{\hat{\psi}_1 - \hat{\alpha}_1} \mathbf{T}_{-\hat{\beta}_1} \begin{bmatrix} \widetilde{\Delta\phi}_0 \\ \widetilde{\Delta\theta}_0 \\ \widetilde{\Delta\psi}_0 \end{bmatrix}. \tag{18}$$

Finally, the previous measurements $\hat{\alpha}_1, \ldots, \hat{\phi}_1$ are updated by adding the incremental angles $\widetilde{\Delta\alpha}_1, \ldots, \widetilde{\Delta\phi}_1$. Note that in the above equations we use the tilde sign($\tilde{.}$) to denote the approximation of the true value, as will be explained in the next section. One can locate the following possible sources of errors in this algorithm:

1) The assumption that the near-field component only is significant. However, this assumption is justified within the measuring volume recommended by the manufacturer ($<$ 3m) because the carrier frequencies, usually in the range of 7-14 kHz [17], yield wavelengths in the 215-430 m range.
2) The linearization and the approximation of the matrix $\widetilde{\mathbf{R}}$. Note that $\widetilde{\mathbf{R}}$ given in (14) is not equal to the original $\mathbf{R}$ in (12). The authors used $\widetilde{\mathbf{R}}$ to derive formulas to obtain the estimates of the position and orientation as given in (15) and (16). In practice, the measurements are taken from the coils of the sensor whose position and orientation are described by $\mathbf{R}$ not $\widetilde{\mathbf{R}}$. That is why we wrote the formulas in (15) and (16) in terms of $\mathbf{R}$. And that is why we used the tilde sign ($\tilde{.}$) to emphasize the idea that the obtained incremental angles are only estimates of the real ones.
3) Transforming from the tracking to the source frame. The incremental angles $\Delta\alpha_0, \ldots, \Delta\phi_0$ measured in the tracking frame obtained from (16) are transformed by (17) and (18) into the incremental angles $\Delta\alpha_1, \ldots, \Delta\phi_1$ measured in the source frame to be used to update the previous measurements. Although the derivations of the transformation rules in (17) and (18) look logical, and they prove to be good approximations, there are two possible sources of error. First, the singularities of the transfer functions. For the incremental angle $\widetilde{\Delta\alpha}_0$, the transformation is obtained by dividing by $\cos\beta_1$. The authors in [17] stated that alternative formulas must be used when $\beta_1 \approx \pm\frac{\pi}{2}$. Unfortunately, the authors in [17] did not propose any alternative formula. The same can be said about dividing by $\cos\hat{\theta}_1$ to obtain the incremental roll angle $\Delta\widetilde{\phi}_1$. Second, and more significantly, the accumulation of the error resulting from those transformation rules. Consider again the transformation rule in (17), for example. The algorithm cannot divide by the real angle β_1 because it is not known. Instead it must use the latest known value, that is $\widetilde{\beta}_1$. Thus, the error in measuring this angle will propagate through the whole algorithm and accumulate as the time progresses.

Actually, the error due to linearization and transformation, explained in the last two points above, is the topic of this work.

3 Error Analysis: Constant Orientation

In this section, we analyze the error in position measurements, assuming that the orientation of the sensor is kept constant. From here on, we use the tilde sign ($\tilde{.}$) to denote the approximated values. We also use the symbol ϵ_x to denote the error between x and the approximation $\tilde{x}$, for any variable x.

3.1 Mathematical Model of the Error

Let $\dot{\alpha}_1(t)$ and $\dot{\beta}_1(t)$ denote the rate of change of the azimuth and elevation angles, respectively, of the sensor with respect to the source frame. Since the measurements are updated every ΔT_u, the measured rate of change of the azimuth and the elevation angles are given by $(\frac{\widetilde{\Delta\alpha_1}}{\Delta T_u})$ and $(\frac{\widetilde{\Delta\beta_1}}{\Delta T_u})$, respectively. Note that the measured angular velocities are constant over ΔT_u time period, while the real velocities may change over the same period. Let us now define the error in measuring the elevation angle as:

$$\epsilon_{\dot{\beta}_1}(t) = \dot{\beta}_1(t) - \widetilde{\dot{\beta}}_1 = \dot{\beta}_1(t) - \frac{\widetilde{\Delta\beta}_1}{\Delta T_u}, \tag{19}$$

and

$$\epsilon_{\Delta\beta_1}(t) = \Delta\beta_1(t) - \widetilde{\Delta\beta}_1(t). \tag{20}$$

where, in the last equation, we consider $\Delta\beta_1(t) = \int_t^{t+\Delta T_u} \dot{\beta}_1(\tau)d\tau$ to allow for changing velocities. From the basic definitions in (19) and (20) one can obtain the following important result:

$$\epsilon_{\Delta\beta_1}(t) = \Delta\beta_1(t) - \dot{\beta}_1(t)\Delta T_u + \epsilon_{\dot{\beta}_1}(t)\Delta T_u. \tag{21}$$

The result above basically means that the errors in measuring the incremental elevation angle and its rate of change are proportional. Then, the error in measuring the elevation angle can be defined as:

$$\epsilon_{\beta_1}(t) = \beta_1(t) - \widetilde{\beta}_1(t), \tag{22}$$

which can be simplified by using (19) and (20) to:

$$\begin{aligned} \epsilon_{\beta_1}(t) &= \int_0^t \dot{\beta}_1(\tau)d\tau - \sum_{i=1}^{\frac{t}{\Delta T_u}} \widetilde{\Delta\beta_1}(i\Delta T_u) \\ &= \int_0^t \dot{\beta}_1(\tau)d\tau - \frac{1}{\Delta T_u}\int_0^t \widetilde{\Delta\beta_1}(\tau)d\tau \\ &= \int_0^t \epsilon_{\dot{\beta}_1}(\tau)d\tau = \frac{1}{\Delta T_u}\int_0^t \epsilon_{\Delta\beta_1}(\tau)d\tau. \end{aligned} \tag{23}$$

So, our strategy to find the error ϵ_{β_1} goes as follows. First, we find an estimate of $\epsilon_{\dot{\beta}_1}$ from (19). Second, we obtain an estimate of $\epsilon_{\Delta\beta_1}$ from (21). Then, we find ϵ_{β_1} from (23) above. For the azimuth angle we follow exactly the same strategy.

First:

$$\epsilon_{\dot{\alpha}_1}(t) = \dot{\alpha}_1(t) - \widetilde{\dot{\alpha}}_1 = \dot{\alpha}_1(t) - \frac{\widetilde{\Delta\alpha_1}}{\Delta T_u}. \tag{24}$$

Then:

$$\epsilon_{\Delta\alpha_1}(t) = \Delta\alpha_1(t) - \dot{\alpha}_1(t)\Delta T_u + \epsilon_{\dot{\alpha}_1}(t)\Delta T_u. \tag{25}$$

Afterwards, the error in azimuth angle will be determined by:

$$\epsilon_{\alpha_1}(t) = \int_0^t \epsilon_{\dot{\alpha}_1}(\tau)d\tau = \frac{1}{\Delta T_u}\int_0^t \epsilon_{\Delta\alpha_1}(\tau)d\tau. \tag{26}$$

Finally, the error in the measured distance between the source and the sensor can be defined as:

$$\epsilon_\rho(t) = \rho(t) - \tilde{\rho}(t). \tag{27}$$

Note that the estimate of distance $\tilde{\rho}$ according to this algorithm is obtained from (15), and it is not obtained by finding the increments from the previous measurement as is done with the azimuth and elevation angles. Thus, we suffice by finding the error in measuring the distance because the error in its rate of change will not be required.

To this end, we discuss how to obtain estimates of $\epsilon_{\dot{\beta}_1}$ and $\epsilon_{\dot{\alpha}_1}$. In order to do that, we keep in mind that the estimated increments $\widetilde{\Delta\beta_0}$ and $\widetilde{\Delta\alpha_0}$ in (16) depend on the real transformation matrix $\mathbf{R}$ in (12) not its approximation $\widetilde{\mathbf{R}}$ in (14), as explained before. Besides, the transformation matrix $\mathbf{R}$ results from the sequence of rotations between the real position (not the measured position) at time t and that at $t + \Delta T_u$. So, we need to distinguish between the previous real position defined by the coordinates $(\hat{\rho}, \hat{\alpha}_1, \hat{\beta}_1) = (\rho(t - \Delta T_u), \alpha_1(t - \Delta T_u), \beta_1(t - \Delta T_u))$, and the previous measured coordinates denoted, from here on, by $(\widetilde{\hat{\rho}}, \widetilde{\hat{\alpha}}_1, \widetilde{\hat{\beta}}_1)$.

3.2 Error Realization

We have the recipe now to find the error. Let us assume that the elevation, azimuth and range of the sensor are changing at the rates $\dot{\beta}_1$, $\dot{\alpha}_1$ and $\dot{\rho}$, respectively. Then, we find the real increment $\widetilde{\Delta\beta_0}$ from (16) and (17) by using the real $\mathbf{R}$ in (12) and substitute in (19).

Actually, even with Symbolic Math Toolbox in MATLAB, obtaining formulas for the above error would not be trivial, and the obtained formulas will be so long to be inserted here. However, with some trigonometry and some approximations one can obtain:

$$\begin{aligned}\epsilon_{\dot{\beta}_1}(t) = \dot{\beta}_1(t) &- \frac{\sin(2\Delta\beta_1)\cos(\Delta\alpha_1)}{\Delta T_u \kappa(t)} \\ &- \frac{\sin(2\beta_1)\sin^2(\Delta\alpha_1)}{2\Delta T_u \kappa(t)},\end{aligned} \tag{28}$$

where

$$\kappa(t) = 2 - 3\sin^2(\Delta\beta_1) - 3\cos^2\beta_1\cos^2\hat{\beta}_1\sin^2(\Delta\alpha_1), \tag{29}$$

and

$$\begin{aligned}\Delta\beta_1(t) &= \int_t^{t+\Delta T_u} \dot{\beta}_1(\tau)d\tau \\ \Delta\alpha_1(t) &= \int_t^{t+\Delta T_u} \dot{\alpha}_1(\tau)d\tau.\end{aligned} \tag{30}$$

Our simulations show that, when the rate of change of the distance $\dot{\rho}$ is not so high, the factor $\kappa(t)$ above can be approximated by 2, and hence:

$$\begin{aligned}\epsilon_{\dot{\beta}_1}(t) = \dot{\beta}_1(t) &- \frac{\sin(2\Delta\beta_1)\cos(\Delta\alpha_1)}{2\Delta T_u} \\ &- \frac{\sin(2\beta_1)\sin^2(\Delta\alpha_1)}{4\Delta T_u},\end{aligned} \tag{31}$$

which yields when inserted in (21):

$$\begin{aligned}\epsilon_{\Delta\beta_1}(t) = \Delta\beta_1(t) &- \frac{\sin(2\Delta\beta_1)\cos(\Delta\alpha_1)}{2} \\ &- \frac{\sin(2\beta_1)\sin^2(\Delta\alpha_1)}{4}.\end{aligned} \tag{32}$$

Finding the error in measuring the elevation angle $\epsilon_{\beta_1}(t)$ requires finding the integral in (23) analytically, and that is tedious. However, numerical evaluation of that integral will do the job, as will be shown in the simulations part. Analogously, finding the real increment $\widetilde{\Delta\alpha_0}$ from (16) and (17) by using the real $\mathbf{R}$ in (12), substituting it in (24) and with the help of Symbolic Math Toolbox in MATLAB, the error in measuring azimuth rate of change reads:

$$\epsilon_{\dot{\alpha}_1}(t) = \dot{\alpha}_1(t) - \frac{2\sin(\Delta\alpha_1)\cos(\Delta\beta_1)}{\Delta T_u \kappa(t)}. \tag{33}$$

In fact, the formula above does not take into consideration the problem of the error propagation explained earlier. To elaborate, the incremental angles $\Delta\alpha_0$ in the tracking frame are transformed to $\Delta\alpha_1$ in the source frame by dividing by $\cos(\beta_1)$ as shown in (17). However, the algorithm can not use the real value of β_1 because it is not available. Instead, the algorithm must use the approximation $\widetilde{\beta}_1$. Thus, the errors $\epsilon_{\dot{\alpha}_1}(t)$ and $\epsilon_{\Delta\alpha_1}(t)$ may explode when the error in measuring the angle β_1 accumulates. In order to take this accumulation into consideration, we propose to modify the formula in (33) into:

$$\epsilon_{\dot{\alpha}_1}(t) = \dot{\alpha}_1(t) - \frac{\sin(\Delta\alpha_1)\cos(\Delta\beta_1)\cos(\beta_1)}{\Delta T_u\cos(\widetilde{\beta}_1)}. \tag{34}$$

Note here also that the factor $\kappa(t)$ in the above formula is approximated by 2 as was done in (31). Now, we need to find an expression for $\widetilde{\beta}_1$ in terms of the real velocities and angles. To this end, we use the error ϵ_{β_1} defined in (22). Thus, the error $\epsilon_{\dot{\alpha}_1}(t)$ can be described by:

$$\epsilon_{\dot{\alpha}_1}(t) = \dot{\alpha}_1(t) - \frac{\sin(\Delta\alpha_1)\cos(\Delta\beta_1)\cos(\beta_1)}{\Delta T_u\cos(\beta_1 - \epsilon_{\beta_1})}. \tag{35}$$

Inserting (35) in (25) results in:

$$\epsilon_{\Delta\alpha_1}(t) = \Delta\alpha_1(t) - \frac{\sin(\Delta\alpha_1)\cos(\Delta\beta_1)\cos(\beta_1)}{\cos(\beta_1 - \epsilon_{\beta_1})}. \tag{36}$$

One more time, we use numerical integration to find the error $\epsilon_{\alpha_1}(t)$ in (26). Finally, the error ϵ_ρ can be determined by finding $\tilde{\rho}$ from (15) by using the real $\mathbf{R}$ in (12) and substituting it in (27). With the help of Symbolic Math Toolbox in MATLAB and some algebraic manipulation, the error is described by:

$$\epsilon_\rho(t) = \rho(t)\left(1 - \sqrt{[3]}\frac{2}{\kappa(t)}\right). \tag{37}$$

Note that if we approximate $\kappa(t)$ by 2 as was done before, the error ϵ_ρ will be zero. When we present our simulations in the subsequent section, we will see that ϵ_ρ is much less than the other errors, as expected from the formula above. However, we keep the factor $\kappa(t)$ for the sake of completeness and to check our model.

The following can be stated about the given formulas:

1) As $\Delta T_u \to 0$, $\Delta\alpha_1 \to \Delta\beta_1 \to 0$, and thus it can be easily shown that:

$$\begin{aligned}&\lim_{\Delta T_u \to 0} \epsilon_{\dot\beta_1}(t) = \lim_{\Delta T_u \to 0} \epsilon_{\Delta\beta_1}(t) = \lim_{\Delta T_u \to 0} \epsilon_{\beta_1}(t) = \\ &\lim_{\Delta T_u \to 0} \epsilon_{\dot\alpha_1}(t) = \lim_{\Delta T_u \to 0} \epsilon_{\Delta\alpha_1}(t) = \lim_{\Delta T_u \to 0} \epsilon_{\alpha_1}(t) = \\ &\lim_{\Delta T_u \to 0} \epsilon_\rho(t) = 0\end{aligned} \tag{38}$$

2) The errors $\epsilon_{\dot\alpha_1}$, $\epsilon_{\Delta\alpha_1}$ and ϵ_{α_1} escape to $\pm\infty$ whenever $\beta_1 - \epsilon_{\beta_1} = \pm(2n+1)\frac{\pi}{2}$ because of the factor $\cos(\beta_1 - \epsilon_{\beta_1})$ placed in the denominator in (35) to account for the error propagation.
3) The errors in the azimuth and elevation measurements do not depend on the distance $\rho(t)$.
4) The above formulas were obtained assuming that the measurements are updated every ΔT_u. In practice, longer time intervals can be experienced. Some time is needed for the data processing. Also some time gap is allocated for taking the measurements, especially if multiplexing is used to distinguish the outputs of the three excitation states, as explained before. Should more precise estimations of the errors be required, the above formulas can be modified by increasing ΔT_u to account for those time gaps, assuming that we can obtain good estimations of them.

3.3 Numerical Simulations

For simulation purposes, the *real* position of the sensor was modeled as follows:

$$\begin{bmatrix}\rho(t+\delta t)\\ \alpha_1(t+\delta t)\\ \beta_1(t+\delta t)\end{bmatrix} = \begin{bmatrix}\rho(t)\\ \alpha_1(t)\\ \beta_1(t)\end{bmatrix} + \begin{bmatrix}\dot\rho(t)\\ \dot\alpha_1(t)\\ \dot\beta_1(t)\end{bmatrix}\delta t, \tag{39}$$

where δt was assumed one tenth of ΔT_u the update time that was assumed $\frac{1}{240}$s as given in the specifications of Polhemus. The initial position of the sensor was assumed at $(\rho_0, \alpha_0, \beta_0) = (0.5, 0, 0)$. The *measured* position was found by the algorithm described in [17], specifically by using (15), (16) and (17), by using the real transformation matrix $\mathbf{R}$ in (12). The initial measured position was assumed as same as the real initial position to avoid the problem of the algorithm initiation and convergence. The errors were measured by taking the difference between the real and the measured positions. Then, the error $\epsilon_\rho(t)$ was calculated by the proposed formula in (37). The error $\epsilon_{\beta_1}(t)$ was determined by integrating $\epsilon_{\dot\beta_1}(t)$ obtained from (28). Finally, the error $\epsilon_{\alpha_1}(t)$ was obtained by integrating the error $\epsilon_{\dot\alpha_1}(t)$ found by using (35). Whether measured or calculated, the errors $\epsilon_{\alpha_1}(t)$ and $\epsilon_{\beta_1}(t)$ can reach values much greater than 2π. So, we subtracted the complete rotations of $2n\pi$ from those errors. The rates of change $\dot\alpha_1(t)$, $\dot\beta_1(t)$, and $\dot\rho(t)$ were assumed to vary as:

$$\begin{aligned}\dot\alpha_1(t) &= B_{\alpha_1} + A_{\alpha_1}\sin(A_{\alpha_1} t)\\ \dot\beta_1(t) &= B_{\beta_1} + A_{\beta_1}\sin(A_{\beta_1} t)\\ \dot\rho(t) &= B_\rho + A_\rho\sin(10\pi t)\end{aligned} \tag{40}$$

where A_{α_1}, B_{α_1}, A_{β_1}, B_{β_1}, A_ρ B_ρ are constants. Three examples were solved. The values of the used constants in each example are listed in Table 2. The examples listed the table were chosen to illustrate the efficiency of the proposed formulas in as different cases as possible within the allowed page limits. In all examples the range ρ was assumed changing at the same rate. This range rate was assumed more complicated (sinusoidal and DC) than the other rates.

TABLE 2
Parameters Used for the Two Examples

	Example I	Example II	Example III
A_{α_1} (rad/s)	10π	0	8.5π
B_{α_1} (rad/s)	0	0	0
A_{β_1} (rad/s)	0	0	1.5π
B_{β_1} (rad/s)	0	10π	0
A_ρ (m/s)	0.2	0.2	0.2
B_ρ (m/s)	0.3	0.3	0.3

The results obtained from solving Example I, Example II and Example III are depicted in Figs. 1, 2 and 3, respectively.

3.3.1 Example I

In this example, $\dot\beta_1$ was assumed zero, as if the sensor does not change its elevation. Thus, the error $\epsilon_{\beta_1}(t)$ was obtained to be zero whether by measuring or by using the proposed formulas. The azimuth rate was assumed pure sinusoidal. As you can see in Fig. 1a, the calculated and measure errors of the range ϵ_ρ coincide. Keep in mind that ϵ_ρ depends on $\kappa(t)$ which is a function of the azimuth and elevation from (29). Since the elevation was assumed constant, $\kappa(t)$ is a function of the azimuth only which in turn was assumed changing sinusoidally. That explains the sinusoidal nature of the error ϵ_ρ. Further, the magnitude of ϵ_ρ is increasing because it depends on $\rho(t)$ as you can see in (37), and $\rho(t)$ was assumed increasing. Moreover, we can note that the magnitude of ϵ_ρ is insignificant, in general. The reason behind that is the fact that $\kappa(t)$ is very close to 2, and this makes the error almost zero, as noted before. On the other hand, Fig. 1b depicts the error $\epsilon_{\alpha_1}(t)$. We can see that the measured and calculated errors do not coincide completely.

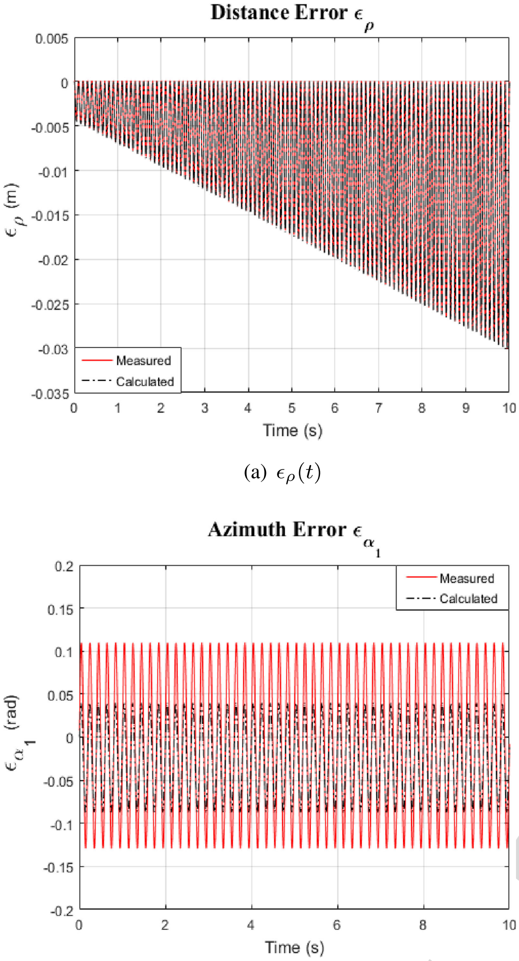

(a) $\epsilon_\rho(t)$

(b) $\epsilon_{\alpha_1}(t)$

Fig. 1. The errors obtained for Example I: (a) $\epsilon_\rho(t)$ (b) $\epsilon_{\alpha_1}(t)$. Measured (solid red) and calculated from the proposed formulas (dotted-dashed black). The measured and the calculated error $\epsilon_{\beta_1}(t)$ were obtained to be zero.

That is because the proposed formulas give an estimate of the error. However, considering the high rate of change assumed for the azimuth in this example, the results can be considered satisfactory, at least to predict the rate of change of the error.

3.3.2 Example II

In this example, the azimuth was assumed fixed ($\dot{\alpha}_1(t) = 0$), and hence the error $\epsilon_{\alpha_1}(t)$ was obtained to be zero whether by measuring or by using the proposed formulas. The elevation was assumed changing at a constant rate ($\dot{\beta}_1(t) = 10\pi$), and the rate of the range was assumed as in Example I. Fig. 2a shows the measured and calculated error ϵ_ρ. One more time, both errors coincide. In addition, we notice that the error is changing steadily because $\dot{\beta}_1$ is constant. The increase in the magnitude is due to the increase of ρ, as explained earlier in Example I. On the other hand, Fig. 2b depicts the error $\epsilon_{\beta_1}(t)$. Obviously, the error is increasing steadily because $\dot{\beta}$ was assumed constant. The estimated error in this case does not coincide completely with the measured error, because the proposed formulas give merely an estimate of this error. However, we claim that the results are satisfactory, especially if the rate of change is not so high.

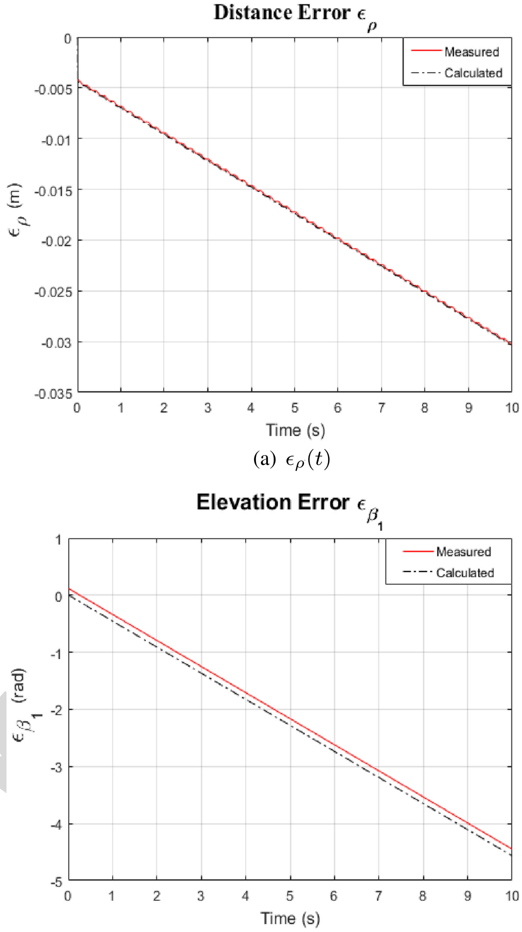

(a) $\epsilon_\rho(t)$

(b) $\epsilon_{\beta_1}(t)$

Fig. 2. The errors obtained for Example II: (a) $\epsilon_\rho(t)$ (b) $\epsilon_{\beta_1}(t)$. Measured (solid red) and calculated from the proposed formulas (dotted-dashed black). The measured and calculated error $\epsilon_{\alpha_1}(t)$ were obtained to be zero.

3.3.3 Example III

This example represents a worse situation in which the position of the sensor changes in all coordinates, and the rates of change $\dot{\alpha}_1(t)$ and $\dot{\beta}_1(t)$ were both assumed of sinusoidal nature. One can see in Fig. 3 that the measured errors $\epsilon_\rho(t)$ and $\epsilon_{\beta_1}(t)$ almost coincide with the calculated values. However, the measured and calculated values of the error $\epsilon_{\alpha_1}(t)$ do not coincide, in general. Deeper look at Fig. 3b shows that the traces of the measured and calculated error $\epsilon_{\alpha_1}(t)$ differ only at the discontinuities or jumps. Those jumps take place when the error changes abruptly by large values or when it exceeds 2π because we subtract the full rotations. This results from the error propagation phenomenon explained earlier and modeled by the factor $\cos(\beta_1 - \epsilon_{\beta_1})$ in the denominator in (35). Thus, whenever the quantity $\beta_1 - \epsilon_{\beta_1} \to \pm(2n+1)\frac{\pi}{2}$ from the left or the right, a jump will occur. Apparently, the magnitude of each jump differs between the calculated and the measured values because the reciprocal of the factor $\cos(\beta_1 - \epsilon_{\beta_1})$ is so sensitive around the singularities. Here, let us remember that the azimuth error $\epsilon_{\alpha_1}(t)$ is calculated by integrating the error $\epsilon_{\dot{\alpha}_1}(t)$ as in (26). The integration thus adds to the randomness of those jumps. In order to illustrate the previous argument, see Fig. 4 that shows the measured and the calculated values of the error in the rate of change of the azimuth angle

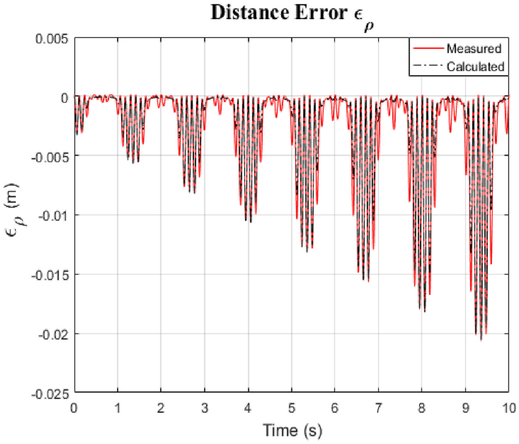

(a) $\epsilon_\rho(t)$

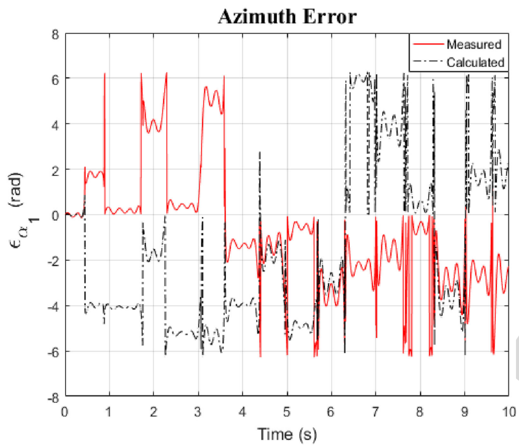

(b) $\epsilon_{\alpha_1}(t)$

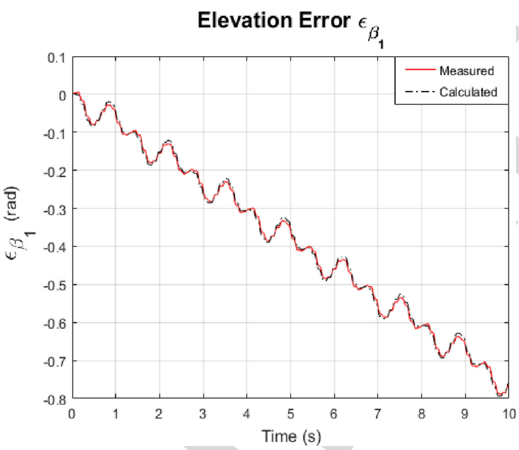

(c) ϵ_{β} (t)

Fig. 3. The errors obtained for Example III: (a) $\epsilon_\rho(t)$ (b) $\epsilon_{\alpha_1}(t)$ and (c) $\epsilon_{\beta_1}(t)$. Measured (solid red) and calculated from the proposed formulas (dotted-dashed black).

$\epsilon_{\dot{\alpha}_1}(t)$ for Example III. Obviosly, the measured and calculated values of the error $\epsilon_{\dot{\alpha}_1}(t)$ coincide except at the discontinuities around the singularities. This, in addition to the integration and randomness of the jump, explains the difference between the measured and calculated values of the error $\epsilon_{\alpha_1}(t)$.

In conclusion, we showed that the proposed formulas can predict the errors with very good accuracy. As the speed of the sensor increases, the results obtained from the proposed formulas diverge from the real values, especially around the singularities where random jumps are encountered. In any case, the proposed formulas can predict the times of those jumps but not their magnitudes. Furthermore, we note that the accuracy of the used algorithm is not as reliable as expected. To elucidate, note that the errors are increasing with time and exploding in some moments (around singularities) although the rates of change of the azimuth and elevation angles were assumed in all examples less than 10π rad/s, namely 5 Hz. However, one can thank that this can be sufficient for biomechanical movements.

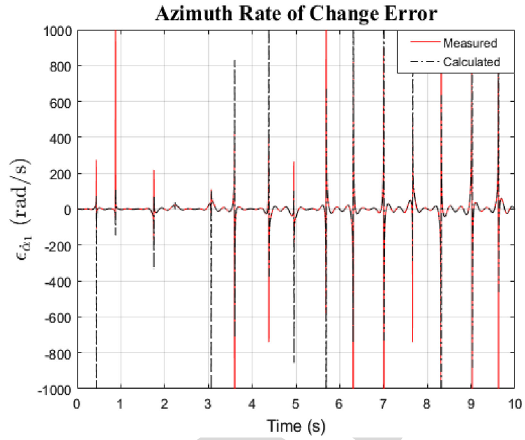

Fig. 4. The error in the azimuth rate of change $\epsilon_{\dot{\alpha}_1}(t)$ obtained for Example III. Measured (solid red) and calculated from the proposed formulas (dotted-dashed black).

4 Varying Orientation

In the previous section, we analyzed the errors in measuring the position of the sensor assuming the orientation constant. Unfortunately, quantifying the errors in orientation measurements is more complicated than describing the errors in position measurements. Assuming the position is constant may look like a good start. Even with this assumption, describing the errors in orientation measurements could be infeasible not only due to the complexity of the transformation matrix $\mathbf{R}$ in (12), but also due to the complex rules in (18) that are used to transform the incremental measured Euler angles from the tracking frame to the source frame and the error propagation encountered with these rules. However, two important results can be drawn about the orientation measurements from the numerical simulations. First, the errors in measuring the orientation is significant even when the position is assumed fixed, and they can be larger than the errors in measuring the position. Let us consider, for example, a sensor which changes its orientation as:

$$\dot{\psi}_1(t) = \dot{\theta}_1(t) = \dot{\phi}_1(t) = 2\pi \sin(2\pi t). \tag{41}$$

For simulation purposes, the *real* orientation of the sensor was modeled as follows:

$$\begin{bmatrix} \psi_1(t+\delta t) \\ \theta_1(t+\delta t) \\ \phi_1(t+\delta t) \end{bmatrix} = \begin{bmatrix} \psi_1(t) \\ \theta_1(t) \\ \phi_1(t) \end{bmatrix} + \begin{bmatrix} \dot{\psi}_1(t) \\ \dot{\theta}_1(t) \\ \dot{\phi}_1(t) \end{bmatrix} \delta t, \tag{42}$$

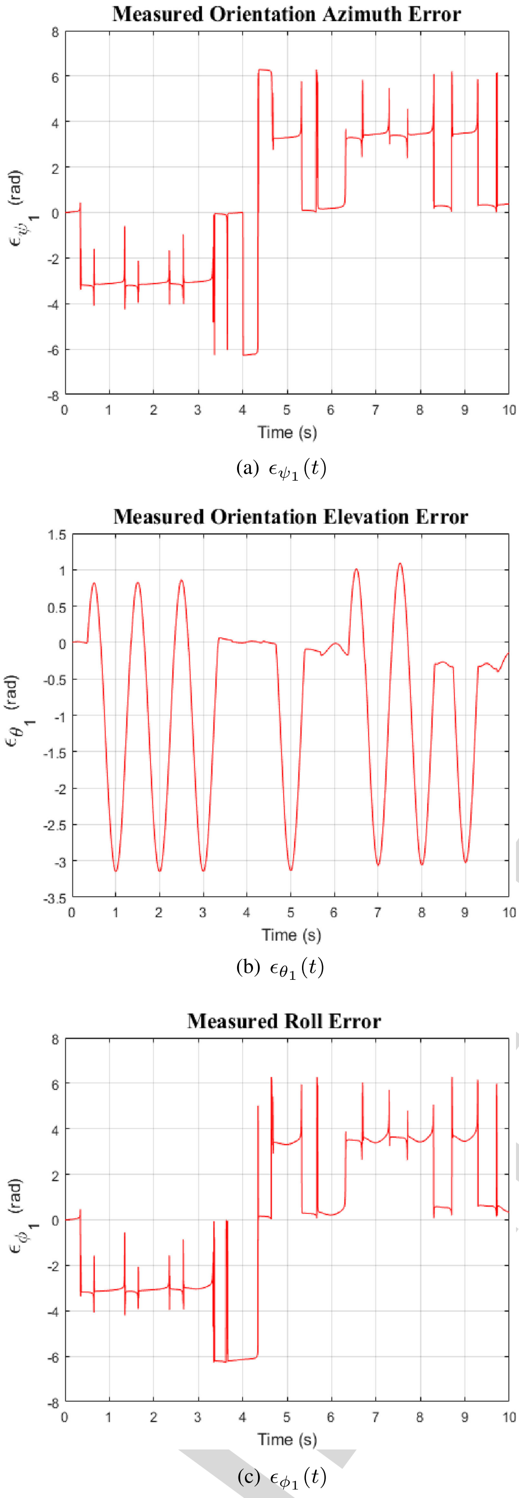

Fig. 5. The errors of orientation measurements when the Euler angles change as in (41) and fixed position: (a) $\epsilon_{\psi_1}(t)$ (b) $\epsilon_{\theta_1}(t)$ and (c) $\epsilon_{\phi_1}(t)$.

where δt was assumed one tenth of ΔT_u, as before. The initial orientation of the sensor was assumed at $(\psi_0, \theta_0, \phi_0) = (0, 0, 0)$. The *measured* orientation was found by the algorithm described in [17], specifically by using (15), (16) and (18), by using the real transformation matrix $\mathbf{R}$ in (12). The initial measured orientation was assumed as same as the real initial orientation. The errors were measured by taking the difference between the real and the measured orientations. Then, a complete rotation of 2π was subtracted whenever the angles exceeded 2π. The results are shown in Fig. 5. Apparently, the orientation errors are changing with time because the Euler angles were assumed changing with time. One can also note that the errors reach levels up to approximately 2π rad although the rate of change of the orientation angles was assumed 2π rad/s i.e., 1 Hz.

The second observation that we could note from our simulations is that the orientation change does not affect the accuracy of the proposed formulas to describe the errors in the position measurements, as long as the rate of change of the orientation is not so large. To illustrate that observation, let us repeat Example III from the previous section by considering changing orientation as in (42). The results are depicted in Fig. 6. Comparing Fig. 3 with Fig. 6, one can note that the difference between the measured and the calculated values of the errors is still small even when the orientation changes. Note also that the error $\epsilon_{\dot{\alpha}_1}(t)$ at fixed orientation from Fig. 3, that was repeated in Fig. 6b for comparison, is still close to the error $\epsilon_{\dot{\alpha}_1}(t)$ at changing orientation, if the jumps around the sigularities are neglected, as explained before. Hence, we can say that the proposed formulas of the errors in position measurements are accurate even when the orientation changes, as long as the rate of change of the orientation is slow.

5 Discussion and Further Work

A natural next step is to empirically verify the suggested model. This could be done by forcing the EMTS through known, dynamic trajectories and comparing the EMTS output to the actual trajectories to quantify the dynamic errors. While conduction of empirical verification is outside the scope of this paper, in the following we give a brief outline of a possible setup and procedure for carrying out this experiment. Ideally, the apparatus used for the experimental investigation will allow the sensor to be moved around the source in all six DOF separately as well as any combinations thereof. A proposed solution is illustrated in Fig. 7. Here, the sensor is attached to the tip of a rigid, non-metallic pylon extending from the distal end of a 6-DOF robot manipulator, said pylon being long enough to allow for the planned sensor trajectories while continually observing the EMTS manufacturer's recommended distances to metallic objects (i.e., the robot).

At any time during the experiment the sensor's 6-DOF position can be deduced from the robot's intrinsic joint sensor outputs and an appropriate kinematic model. If unmodeled elastic deflection of the pylon or the robot itself is a concern, the sensor can be equipped with lightweight, reflective markers and tracked with an optical motion tracking system (Relevant manufacturers of optical motion tracking systems are Vicon, OptiTrack, Qualisys and similar), which will provide ground truth data for the sensor's actual movements. Alternatively, or additionally, the EMTS sensor can be equipped with inertial sensors to provide ground truth data on acceleration and angular velocity. All ground truth data can be combined in e.g., a Kalman filter to provide optimally correct values. The resulting errors of this ground truth system will decide the accuracy of the eventual experimental verification, its magnitude depending on the exact equipment selected; further details on this are outside the

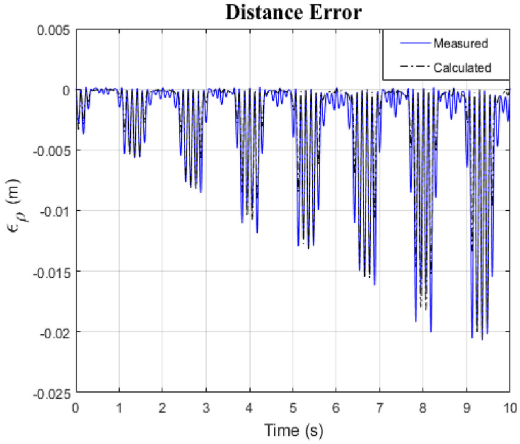

(a) $\epsilon_\rho(t)$

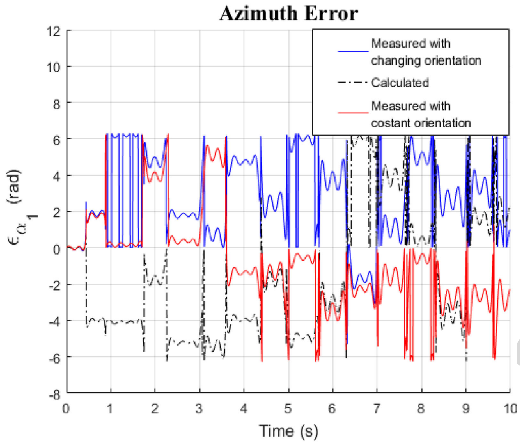

(b) $\epsilon_{\alpha_1}(t)$ (The measured error at fixed orientation obtained in Fig. 3(b) is repeated here in red for comparison)

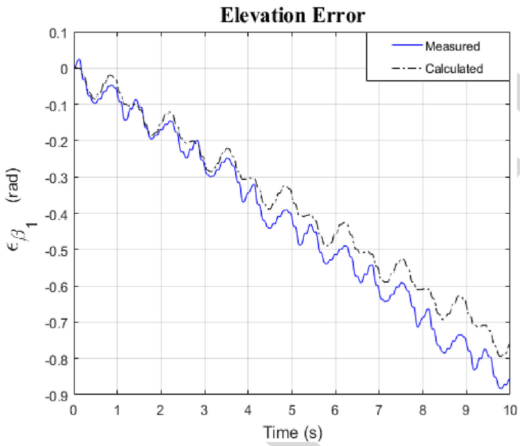

(c) $\epsilon_{\beta_1}(t)$

Fig. 6. The errors obtained for Example III when the orientation changes as in (41): (a) $\epsilon_\rho(t)$ (b) $\epsilon_{\alpha_1}(t)$ and (c) $\epsilon_{\beta_1}(t)$. Measured (solid blue) and calculated from the proposed formulas (dotted-dashed black)

scope of this paper, except to say that equipment of sufficient performance should be readily available. Any applicable calibration of the robot, EMTS and ground truth system should be completed prior to further data acquisition. The robot may then be programmed to put the sensor in different static 6-DOF positions to experimentally establish the overall

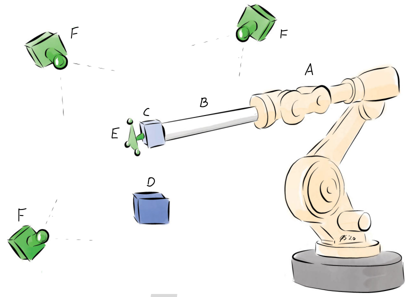

Fig. 7. Suggested experimental setup with robot (A), pylon (B), EMTS sensor (C) and source (D). Optional: reflective marker cluster (E), optical motion tracking cameras (F) and/or sensor mounted inertial sensors (not shown) for ground truth measurements. Components not to scale, number of cameras and markers arbitrary.

system's static accuracy and precision. Finally, the robot is programmed to implement sensor movements such as those simulated in Subsection III.C to experimentally quantify the EMTS' dynamic errors. This can be repeated at different distances from the source and using a range of velocities and accelerations to establish the errors' dependency on these parameters.

6 Conclusion

In this work a theoretical analysis of the dynamic error in position measurements by Polhemus EMTS was performed based on their published algorithm as described in [17]. There are several sources of errors in such systems. The current work discussed one source of the error, in particular the linearization. Formulas to estimate the error in position measurements that results from the sensor motion at fixed orientation in terms of the position and the speed of the sensor in spherical coordinates were derived. Numerical simulations were executed to compare the error estimated by the proposed formulas with the error measured from the simulations. The proposed formulas were given in spherical coordinates, but the corresponding formulas in Cartesian coordinates can be easily found if preferred. In addition, the proposed formulas can be modified by increasing the update time to account for other time gaps such as processing time and multiplexing (if any) time, if more accurate estimates are required. The results of our simulations showed that the proposed formulas are accurate for the error in distance and elevation measurements. The error in azimuth measurement estimated by the proposed formulas did not coincide with the measured one due to the error propagation phenomenon that results in error explosion around the singularities of the transfer function. However, the proposed formulas could predict the singularities. Besides, if the manufacturer measures to avoid the jumps due to these singularities are known, the estimated error by using the proposed formulas would coincided with the measured error. Simulations of varying orientation were also carried out and showed that the error in orientation measurements is, in general, larger than the error in position measurements.

Moreover, the numerical simulations showed that the proposed formulas to estimate the error in position measurements are still acceptable with changing orientation, as long as the rates of change of the Euler angles are not large.

The proposed formulas predict that the error increases with motion, in general. In addition, they imply that the error explodes around the singularities of the transfer function. Those conclusions were confirmed by the simulations. This, however, does not mean that Polhemus EMTS are unreliable. Those conclusions imply that some preventive measures are taken to compensate for this type of error, e.g redundancy of sensors. Unfortunately, since the manufacturers are discreet about the details of their algorithm, we can not be sure. In any case, the proposed formulas can be used by the manufacturers to improve their system and by any researcher who is interested in a profound error analysis. Besides, this error model applies to any algorithm of motion detection that exploits similar method of linearization.

REFERENCES

[1] A. M. Franz, T. Haidegger, W. Birkfellner, K. Cleary, T. M. Peters and L. Maier-Hein, "Electromagnetic tracking in medicine – a review of technology, validation and applications," *IEEE Trans. Med. Imag.*, vol. 33, no. 8, pp. 1702–1725, Aug. 2014.

[2] K. Kobayashi, L. Gransberg, E. Knutsson and P. Nolen, "A new system for three-dimensional gait recording using electromagnetic tracking," *Gait Posture*, vol. 6, pp. 63–75, 1997.

[3] K. N. An, M. C. Jacobsen, L. J. Berglund, and E. Y. S. Chao, "Application of A magnetic tracking device to kinesiological studies," *J. Biomechanics*, vol. 21, no. 7, pp. 613–620, 1988.

[4] M. Field, D. A. Stirling, F. Naghdy, and Z. Pan, "Motion capture in robotics review," in *Proc. IEEE Int. Conf. Control Autom.*, 2009, pp. 1697–1702.

[5] G. Welch and E. Foxlin, "Motion tracking: No silver bullet, but a respectable arsenal," *IEEE Comput. Graphics Appl.*, vol. 22, no. 6, pp. 24–38, Nov./Dec. 2002.

[6] V. V. Kindratenko, "A survey electromagnetic position tracker calibration techniques," *Virt. Reality*, vol. 5, pp. 169–182, 2000.

[7] H. P. Kalmus, "A new guiding and tracking system," *IRE Trans. Aerosp. Navigational Electronics*, vol. ANE-9, no. 1, pp. 7–10, Mar. 1962.

[8] J. E. Lenz, "A review of magnetic sensors," in *Proc. IEEE*, vol. 78, no. 6, pp. 973–989, Jun. 1990.

[9] S. Bryston, "Measurement and calibration of static distortion of position data from 3D trackers," *Proc. SPIE, Stereoscopic Displays Appl. III*, vol. 1669, pp. 244–255, Jun. 1992.

[10] J. Hummel, M. Figl, M. Bax, R. Shahidi, H. Bergmann and W. Birkfellner, "Evaluation of dynamic electromagnetic tracking deviation," in *Proc. SPIE Med. Imag., Vis. Image-Guided Procedures Model.*, 2009, vol. 7261.

[11] M. J. Murphy, R. Eidens, E. Vertatschitsch and J. N. Wright, "The effect of transponder motion on the accuracy of the Calypso electromagnetic localization system," *Int. J. Radiat. Oncol. Biol. Phys.*, vol. 72, no. 1, pp. 295–299, 2008.

[12] M. A. Nixon, B. C. McCallum, W. R. Fright and N. B. Price, "The effects of metals and interfering fields on electromagnetic trackers," *Presence*, vol. 7, no. 2, pp. 204–218, Apr. 1998.

[13] F. H. Raab, "Quasi-static magnetic-field technique for determining position and orientation," *IEEE Trans. Geosci. Remote Sens.*, vol. GE-19, no. 4, pp. 235–243, Oct. 1981.

[14] A.-K. Stensdotter, M. DinhoffPedersen, I. Meisingset, O. Vasseljen, and Ø. Stavdahl, "Mechanisms controlling human head stabilization during random rotational perturbations in the horizontal plane revisited," *Physiol. Rep.*, vol. 4, no. 10, 2016, Art. no. e12745.

[15] [Online]. Available: http://polhemus.com/motion-tracking/all-trackers/liberty

[16] [Online]. Available: http://www.polhemus.com/

[17] F. H. Raab, E. B. Blood, T. O. Steiner and H. R. Jones, "Magnetic position and orientation tracking system," *IEEE Trans. Aerosp. Electronic Syst.*, vol. AES-15, no. 5, pp. 709–718, Sep. 1979.

[18] J. B. Kuipers, "SPASYN-an electromagnetic relative position and orientation tracking system," *IEEE Trans. Instrum. Meas.*, vol. IM-29, no. 4, pp. 462–466, Dec. 1980.

Mutaz Tuffaha received the BSc degree in electrical engineering from the University of Jordan, in 1999, the MSc degree in signal processing, and another MSc degree in mathematics from Linnaeus University, Sweden, in 2011 and 2012, respectively, and the PhD degree in engineering cybernetics from the the Norwegian University of Science and Technology (NTNU), Norway, 2016. Then, he joined the Department of Neuromedicine and Movement Science, NTNU, as a postdoc research fellow conducting his research on motion tracking systems and gait analysis. Currently, He is an algorithm developer at Indra Navia AS in Norway working on augmented landing systems. His research interests include: control systems, signal processing, motion tracking, data analysis, optimization and GPS.

Øyvind Stavdahl received the MSc and PhD degrees from the Department of Engineering Cybernetics, Norwegian University of Science and Technology (NTNU), Trondheim, Norway, in 1994 and 2002, respectively. He became a research scientist, in 1998, and a senior scientist, in the Department of Applied Cybernetics, SINTEF Information and Communication Technology, in 2004, where he headed the Motion Control research Group for a time. Following a period as a postdoctoral fellow and lecturer, he became an associate professor in 2008, and professor in the Department of Engineering Cybernetics, NTNU, in 2018. He was a visiting fellow with the Institute of Biomedical Engineering, University of New Brunswick, Fredericton, NB, Canada, in 2005, he was a visiting academic in Auckland Bioengineering Institute in Auckland, New Zealand, during 2017-2018 . He was a co-founder of Cypromed, a Norwegian start-up company that pioneered the use of Li-ion batteries in upper-limb prostheses in the late 1990'ies, and he is presently a co-founder and scientific advisor of the subsea robotics company Eelume. His many research interests include rehabilitation engineering and biomimetic robotics.

Ann-Katrin Stensdotter receoived the PhD degree in physiotherapy specializing in movement science, from Umeå University, Sweden. She is currently a full professor with the Norwegian University of Science and Technology (NTNU), and has been teaching basic science at the physiotherapy program at NTNU, since 1997. Her major work has been conducted in laboratory settings investigating movement issues in various conditions, with special focus on effects of long-standing pain. Her research interest include human movement science, human motor control using methods of 3D kinematics, kinetics and electromyography in studies of movements, and forces and muscle activity. The objective is foremost to understand movement anomalies and derive underlying mechanisms that may explain strategies or deficits in motor control such as postural control and gait.